On the potential of variational calibration for a fully distributed hydrological model: application on a Mediterranean catchment

Maxime Jay-Allemand[1,2], Pierre Javelle[1], Igor Gejadze[2], Patrick Arnaud[1], Pierre-Olivier Malaterre[2], Jean-Alain Fine[3], and Didier Organde[3]

[1]INRAE, Aix Marseille Université, RECOVER, 3275 Route de Cézanne, Aix-en-Provence, 13182, France
[2]INRAE, UMR G-EAU, 361 rue Jean-François Breton, 34196 Montpellier, France
[3]Hydris-Hydrologie, Parc Scientifique Agropolis II, 2196 Boulevard de la Lironde, 34980 Montferrier sur Lez, France

Correspondence: Maxime Jay-Allemand (maxime.jay-allemand@inrae.fr)

Abstract. Calibration of a conceptual distributed model is challenging due to a number of reasons, which include fundamental (model adequacy, identifiability) and algorithmic (e.g. local-search versus global-search) issues. The aim of the presented study is to investigate the potential of the variational approach for calibrating a simple continuous hydrological model (GRD) involved in several flash-flood modelling applications. This model is defined on a rectangular $1\,km^2$ resolution grid, with three parameters being associated to each cell. The Gardon d'Anduze watershed ($543km^2$) is chosen as the study benchmark. For this watershed, the discharge observations at five gauging stations, gridded rainfall and potential evapotranspiration estimates are continuously available for the 2007-2018 period at an hourly time step.

In the variational approach one looks for the optimal solution by minimizing the standard quadratic cost-function which penalizes the misfit between the observed and predicted values, under some additional a-priori constraints. The cost-function gradient is efficiently computed using the adjoint model. In numerical experiments, the benefits of using the distributed against the uniform calibration are measured in terms of the model predictive performance, in temporal, spatial and spatio-temporal validation, both globally and for particular flood events. Overall, distributed calibration shows encouraging results, providing better model predictions and relevant spatial distribution of some parameters. The numerical stability analysis has been performed to understand the impact of different factors on the calibration quality. This analysis indicates the possible directions for future developments, which may include considering a non-gaussian likelihood and upgrading the model structure.

Keywords : fully distributed rainfall-runoff model, calibration, variational data assimilation, adjoint model

1 Introduction

Flash flood prediction remains a challenging task of modern hydrology due to a number of reasons. First, the heavy precipitation events (HPEs) leading to flash floods are difficult to forecast due to complexity of the processes involved (deep convection triggered by orographic lifting, low level wind convergence and/or cold pools (Ducrocq et al., 2016). Second, the hydrological response of the watershed is difficult to model, since it depends on many factors. These include the watershed properties (topography, geology, land-cover) and its initial state, for example the soil moisture (Braud et al., 2016). For the Western Mediterranean region which is often affected by flash floods, the HyMeX program (Hydrological Cycle in the Mediterranean Experiment) offers a good opportunity to conduct multi-disciplinary studies on the relevant subjects (Drobinski et al., 2014).

In order to better predict flash floods and reduce their potentially devastating impact, warning systems have been developed or are currently under development (Collier, 2007; Hapuarachchi et al., 2011; Gourley et al., 2017). The distributed hydrological models utilizing the rainfall radar measurements are widely implemented in such systems. These models take into account the spatial variability of the catchment properties and of the rainfall, and are capable of predicting the discharge at ungauged locations. The latter is important for small-/medium-sized watersheds which are not covered by an extensive gauging network (Borga et al., 2011). Among operational models presently used for flash flood prediction at a national scale one could mention the CREST model in the USA developed by Wang et al. (2011) or the G2G model (UK) from Bell et al. (2007). Those distributed models are often 'conceptual', because considering more complex 'physically-based' models may not be justified for the flash flood prediction purpose (Beven, 1989). Since the conceptual parameters are not directly observable, they have to be defined using calibration. However, due to a potentially significant number of cells or sub-catchments, the calibration process have to deal with over-parametrisation and uniqueness (equifinality) issues (Beven, 1993, 2001). Another set of difficulties stems from a dubious adequacy of such models, in which case the very definitions of 'over-parametrisation' and 'over-fitting' should be refined.

As noticed in De Lavenne et al. (2019), all existing calibration methods developed for the distributed hydrological models involve some sort of regularization strategy. One possible approach is the control set reduction. For example, for each distributed parameter one can try to evaluate a non-uniform spatial pattern from information about the catchment characteristics, including its geological formation, soil properties and land use (Anderson et al., 2006). Then, instead of calibrating the local values of parameters associated to each grid cell, one calibrates a few 'superparameters' (additive constant, multiplier, power) that modify this pattern according to a chosen law, see e.g. Pokhrel and Gupta (2010). The same idea but in the multiscale setting is implemented in the multiscale parameter regionalization (MPR) method described in Samaniego et al. (2010). Other strategies can also include the use of additional data, as in Rakovec et al. (2016), where satellite-based total water storage (TWS) anomaly is used to

complement the discharge data. For a low-dimensional unknown vector one can use a variety of probabilistic or gradient-free methods to find the sought estimate. It has to be recognized, however, that evaluating useful spatial patterns from auxiliary information is a difficult task by itself. In the presented paper we investigate the possibility of calibrating the distributed parameters without considering any pre-defined spatial structures. Such calibration problem falls into the category of high-dimensional inverse problems which can be addressed through the appropriate data assimilation methods.

Methods of data assimilation (DA) have been engaged for several decades in geosciences, including meteorology, oceanography, river hydraulics and hydrology applications. These methods are used for estimating the driving conditions, states and/or parameters (calibration) of a dynamical model describing the evolution of a natural phenomena. The estimates are conditioned on observations (usually incomplete) of a prototype system. Some early applications of DA in hydrology are described in the review paper of McLaughlin (1995). More recently the review paper of Liu et al. (2012) report the progress and challenges of data assimilation applications in operational hydrological forecasting. It seems that the Kalman filtering has been recently the most popular DA method in hydrology (Sun et al., 2016). For instance, in Quesney et al. (2000) the Extended Kalman Filter is applied with a lumped conceptual rainfall-runoff model to estimate the soil moisture by assimilating the SAR (synthetic aperture radar) data. In Munier et al. (2014), the standard Kalman Filter is applied with the semi-distributed conceptual model TGR, where the discharge observations are assimilated to adjust the initial model states. It has been shown that the predictive performance depends on the degree of 'spatialization' of the watershed and on the number of gauging stations engaged. In Sun et al. (2015), the Extended Kalman filter is used with the distributed SWAT model to improve flood prediction on the upstream Senegal river catchment. In this work, given the large number of state variables, only the spatially-averaged low-resolution updates are estimated. This shows that for DA involving distributed models, scalable methods must be used (scalable algorithm is the one able to maintain the same efficiency when the workload grows). The choice of DA methods is, therefore, limited to the Ensemble Kalman Filter and the variational estimation.

In variational estimation, one looks for the minimum of the cost-function dependent on the control vector (i.e. vector of unknown model inputs) using a gradient-based iterative process. The cost-function itself represents the maximum a posteriori (MAP) estimator, which turns into the standard 4D-Var cost-function (Rabier and Courtier, 1992) under the Gaussian assumption. The key issue of variational estimation is the method used for computing the gradient. For low-dimensional control vector the finite-difference approach can be used. For example, Abbaris et al. (2014) explored such variational estimation algorithm involving the lumped conceptual HBV model in operational setting. It has been used to update the soil moisture and the states of the routing tank reservoirs on some events. It has been shown that DA helps to improve the peak flow prediction, however the correct choice of the assimilation period and the forecast horizon is vital. In Thirel et al. (2010), the cost-function is minimized iteratively using the BLUE formulation, which is equivalent to the 'algebraic' form of the Gauss-Newton method. Here, DA is imple-

mented involving the SIM model. It has been shown that the improved estimate of the moisture of the soil layers leads to a significantly better discharge simulation. However, the genuine variational estimation method relies on the adjoint model, which allows the precise (up to round-off errors) gradient of the cost-function to be computed in a single adjoint run. Then, different minimization methods can be applied. For example, in weather/ocean forecast-ing, where the models involved are computationally very expensive, the Gauss-Newton method (e.g. 'incremental approach') is used. This method (as any local search method) leads to a nearest local minimum in the vicinity of the prior guess. This could be a serious problem if the posterior distribution is multimodal. Certain past attempts with the local search methods in hydrology were not always successful and several authors have reported that these methods fail to deliver the global optimal solution (Moradkhani and Sorooshian, 2009; Abbaspour et al., 2007). For high-dimensional, but relatively inexpensive models, the gradient-enhanced global search minimization methods can be considered (Laurent et al., 2019).

Using the variational estimation involving the adjoint is very common in atmospheric and oceanographic appli-cations. But, in hydrology, only a very few cases have been actually reported. In particular, in Castaings et al. (2009) and Nguyen et al. (2016), the adjoint model has been generated/derived for the kinematic wave overland flow model with the source term including the rainfall as a driving condition and the infiltration term described by a Green-Ampt model (Castaings et al., 2009) or the Horton model (Nguyen et al., 2016). Since models are represented by a partial differential equation, this is a standard case for which a significant experience has been accumulated within the data assimilation community. The major difference between the two papers is that in Castaings et al. (2009) the adjoint has been generated by automatic differentiation applied to the existing 'Marine' model, and in Nguyen et al. (2016) - derived and implemented manually. In Castaings et al. (2009) the distributed parameters of the infiltration model has been calibrated considering a single flood event in an identical twin experiment framework, whereas in Nguyen et al. (2016) the author looks for a few global parameters considering two realistic events. In Seo et al. (2009) the adjoint is used for state updating of a lumped model, in Lee et al. (2012) - for state updating of a distributed model.

The aim of our study is to assess a set of parameters which may represent the spatially varying hydrological proper-ties of a chosen watershed; thus the distributed model parameters have to be calibrated over a very long assimilation window (i.e several years). With this purpose we develop a variational calibration method using the adjoint applied on a simple fully distributed model (GRD), involving a conceptual cell-to-cell routing scheme. This scheme has been designed keeping in mind the differentiability requirement. The adjoint is obtained by automatic differentiation and manually optimized to provide the capacity to work for long time periods (up to several consecutive years) over large spatial areas, with fine resolution. This requires a memory efficient and fast code. The distributed parameters of the GRD model are calibrated over a French Mediterranean catchment, the Gardon d'Anduze, using rainfall radar data and the discharge data from the outlet gauge station. The discharge data from other gauge stations available in this

catchment are used for cross-validation (10 years, being split in two periods). Thus, the major questions addressed in this paper are: a) can we, in principle, benefit from considering the spatially distributed set of coefficients given by the method instead of the uniform (homogeneous) set of coefficients and to what extent? In particular, does it help to improve the discharge prediction over the catchment area including 'ungauged' locations? b) What are the major difficulties associated with this approach (insufficient data, structural deficiency of the model, identifiability issue, etc.) and what could possibly be done to improve the model predictive performance?

The paper is organized as follows. In Section 2.1 the GRD model used in this study is described. In Section 2.2 we present the variational estimation algorithm adapted for the parameter calibration purpose. The testing benchmark is described in Section 2.3, and the testing methodology in Section 2.4. The results are presented in Section 3, followed by the Discussion and Conclusions section.

2 Methodology and data

2.1 Distributed rainfall-runoff model GRD

The GRD model (i.e. GR 'distributed') is a conceptual distributed hydrological model designed for flash flood prediction (Javelle et al., 2010; Arnaud et al., 2011; Javelle et al., 2014, 2016). Since March 2017, it is used operationally by the national French flash flood warning system called 'Vigicrues Flash' (Javelle et al., 2019). The model version used in the present study has been specially developed for testing the potential of distributed calibration using the variational approach. It is defined on a regular 1 km^2 grid and runs at hourly time step. For each time step the model input includes the gridded rainfall and potential evapotranspiration, and the output is the discharge field defined at the routing scheme nodes.

Our model incorporates some features from the 'GR' (Génie Rural) models family, which include several lumped and semi-distributed bucket-style continuous models developed over the last 30 years at INRAE-Antony. Those models have been extensively tested and have demonstrated good performances in various conditions and for different time steps (Perrin et al., 2003; Mouelhi et al., 2006; Lobligeois et al., 2014; Ficchì et al., 2016; Santos et al., 2018; Riboust et al., 2019; De Lavenne et al., 2019).

Let us consider a 2D-spatial domain (basin/catchment/watershed) Ω covered by the rectangular grid. For each cell (pixel), the model involves the production and transfer reservoirs, characterized by capacities c_p and c_t, correspondingly, and the discharge generated within each cell is routed between cells with local routing velocity v (see Fig.1). It means only 3 parameters need to be defined for each cell. The integral flow, without distinction between surface, subsurface or groundwater flow, is simulated by the production and transfer reservoirs at the cell level, and by routing scheme at the inter-cell level. Obviously, such model conceptually describes the overall hydrological

process, rather than its physically meaningful components.

The water balance operator:

Let $P(t)$ be the local total rainfall (function of time t), and $E(t)$ - the local total potential evapotranspiration. For each cell (pixel), a water balance function determines the effective rainfall P_r, i.e. the amount of rainfall that will participate to the flow. This function is defined via the following steps. First, the net rainfall P_n and the net potential evapotranspiration E_n are defined from the following equation:

$$\begin{cases} P_n = P - E, \ E_n = 0, & if \ P \geq E, \\ P_n = 0, \ E_n = E - P, & if \ P < E \end{cases}.$$ (1)

Next, the production reservoir is filled by P_p, a part of P_n. Similarly, the production reservoir is emptied by E_p, a part of E_n representing the actual evapotranspiration. The variation of the reservoir level h_p is driven by the following differential equation (Edijatno, 1991):

$$dh_p = \left[1 - \left(\frac{h_p}{c_p} \right)^2 \right] dP_n - \frac{h_p}{c_p} \left(2 - \frac{h_p}{c_p} \right) dE_n.$$ (2)

Assuming a stepwise approximation of input variables $P(t)$ and $E(t)$, equation (2) is integrated over one time step Δt to obtain the amount P_p filling the reservoir and the amount E_p evaporated from it:

$$P_p = c_p \left(1 - \left(\frac{h_p}{c_p} \right)^2 \right) \frac{tanh \left(\frac{P_n}{c_p} \right)}{1 + \left(\frac{h_p}{c_p} \right) tanh \left(\frac{P_n}{c_p} \right)},$$ (3)

$$E_p = h_p \left(2 - \frac{h_p}{c_p} \right) \frac{tanh \left(\frac{E_n}{c_p} \right)}{1 + \left(1 - \frac{h_p}{c_p} \right) tanh \left(\frac{E_n}{c_p} \right)}.$$ (4)

It should be noted that with this discretized temporal formulation, h_p is the reservoir level at the beginning of Δt, P_p and E_p are the volume of water gained or lost by the reservoir over Δt. At the end of Δt, h_p is updated by adding P_p or removing E_p, before progressing to the next time step. Finally, P_r is the part of the net rainfall that does not enter into the production reservoir:

$$P_r = P_n - P_p$$ (5)

One can see, that the state of the production reservoir h_p plays the role of the humidity state of the soil. An empty reservoir ($h_p = 0$) means that the soil is completely dry: effective rainfall and evapotranspiration are equal to zero, and all amount of the net rainfall enters into the production reservoir ($E_p = 0$, $P_p = P_n$, $P_r = 0$). On the contrary, a full reservoir ($h_p = c_p$) means that the soil is completely saturated: no more rainfall enters into the production reservoir, the evapotranspiration is maximal and all the net rainfall produces the effective rainfall ($E_p = E_n$, $P_p = 0$,

$P_r = P_n$).

The transfer operator:

The effective rainfall $P_r(t)$ fills the transfer reservoir characterized by state h_t and capacity c_t. The emission from the transfer reservoir during Δt gives the elementary discharge q. This transformation is modeled by a conservative operator which is derived from the differential equation describing the evolution of h_t under the mass conservation condition:

$$\frac{dh_t}{dt} + c_t h_t^a = P_r, \tag{6}$$

It has been noticed (Perrin et al., 2003) that equation (6) correctly replicates the flooding and drying processes for $a = 5$. This is an empirical knowledge which has no physical justification. Assuming P_r is the impulse function, equation (6) is integrated over one time step Δt to obtain the expression for q:

$$q = h_t - (h_t^{-4} + c_t^{-4})^{-0.25} \tag{7}$$

More details about the production and the transfer reservoirs can be found in (Perrin et al., 2003).

The routing scheme (cell-to-cell):

The total discharge (Q) in a cell is then obtained by routing through the catchment all the upstream elementary discharges (q). This routing is built on top of a digital elevation model which, for a given node, defines the flow direction. The routing nodes are placed at the center of the corresponding cells.

For the sake of simplicity we describe the routing model in the one-dimensional setting. The total discharge from node $i-1$ to node i is delayed by time

$$\tau(v_{i-1,i}) = \frac{d_{i-1,i}}{v_{i-1,i}}, \tag{8}$$

where $d_{i-1,i}$ and $v_{i-1,i}$ are the distance and the routing velocity between the nodes, respectively. In the simplest implementation, the output discharge (more precisely, the mass over the time step Δt) is given as

$$Q_i(t) = q_i(t) + Q_{i-1}(t - \tau(v_{i-1,i})), \tag{9}$$

where Q_i is the total discharge in cell i, Q_{i-1} - the total discharge in the neighbouring upstream cell, and q_i - the elementary discharge emitted from the transfer reservoir over time period δt at cell i. Note that in a 2D case, the second term of the right-hand side of (9) could be a sum of a few contributions from direct neighbouring cells, with their own values of d and v. Since no explicit expression for Q is provided, Q is not differentiable with respect to v. That is why the above formulation is not suitable for variational approach, which requires the gradient of the cost

function to be computed. In order to tackle this issue we represent the second term in equation (9) in the integral form as follows

$$Q_{i-1}(t - \tau(v_{i-1,i})) = \int\limits_{t'=-\infty}^{t} Q_{i-1}(t')\,\delta(t' - \tau(v_{i-1,i}))\,dt'. \tag{10}$$

Next, instead of δ-function we use the unscaled Gaussian function, i.e.

$$5 \quad Q_{i-1}(t - \tau(v_{i-1,i})) = \int\limits_{t'=-\infty}^{t} Q_{i-1}(t')\,\omega\!\left(t' - \frac{d_{i-1,i}}{v_{i-1,i}}, \sigma\right) dt', \tag{11}$$

where

$$\omega(t,\sigma) = exp\left(-\frac{t^2}{2\sigma^2}\right). \tag{12}$$

It is easy to see that function (11) explicitly depends on v_i via ω, therefore the gradient of Q_{i-1} with respect to v_i can be computed. Assuming $Q(t)$ is a constant during a time step period Δt, equation (11) can be written in the
10   discrete form as follows:

$$Q_{i-1}(t - \tau(v_{i-1,i})) = \sum_{l=1}^{L} \bar{\beta}_{i,l}\,Q_{i-1}(t - (l-1)\Delta t), \tag{13}$$

where

$$\bar{\beta}_{i,l} = \beta_{i,l} / \sum_{l=1}^{L} \beta_{i,l},$$

$$15 \quad \beta_{i,l} = w\left(t - (l-1)\Delta t - \frac{d_{i-1,i}}{v_{i-1,i}}, \sigma\right), \; l = 1, \dots, L.$$

and L defines the finite time period (in terms of Δt) instead of the semi-infinite period considered in (10). For the given estimate of routing velocities $v_{i-1,i}$, the coefficients $\beta_{i,l}$ does not change with time and, therefore, can be pre-computed and saved in memory. The spread coefficient σ models the diffusion. The value of parameter σ should not be lower than 0.5 to avoid numerical instability (i.e. when a small variation of the routing velocity results
20   into a large variation of "delay"). Therefore, $\sigma = 0.5$ is used in computations. In terms of using the exponential weights the presented routing model resembles the Lag and Route (LR) model described in (Laganier et al., 2014) and (Tramblay et al., 2010). However, the Gaussian function represents the hydraulic response function in a more realistic way. Indeed, in the Lag and Route method, the kernel function ω is discontinuous, being zero for $t' > t - \tau$. It means the outflow from cell $i-1$ arrives to cell i in a 'shock' manner. If the Gaussian function is used, there is no
25   discontinuity, i.e. outflow from cell $i-1$ arrives to cell i progressively. This scheme is more suitable for cell-to-cell implementation as it is more stable for direct modelling and the absence of discontinuity is a necessary condition to achieve the differentiability of the forward operator.
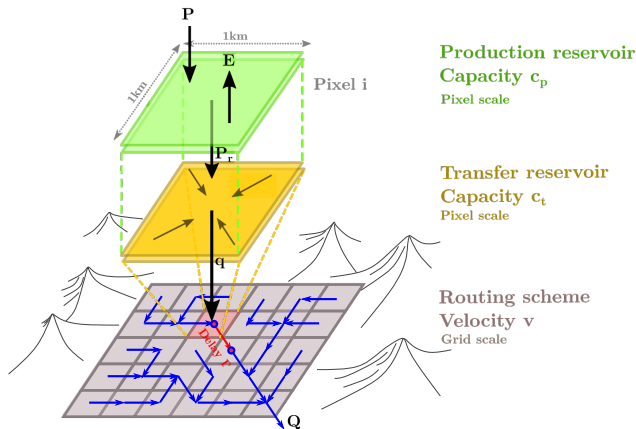
Figure 1. General outlines of the GRD model: P represents the local rainfall over one cell, E - the potential evapotranspiration, P_r - the effective rainfall, q - the elementary discharge and Q - the total routed discharge.

2.2   Variational calibration algorithm

Calibrating a distributed model is often difficult due to a number of reasons. First, the total number of the sought parameters can be quite large (high dimensionality). This strictly limits the choice of suitable inference methodologies. Second, there is an identifiability issue given the sparsity of observations in space, the information content of the test signal (rainfall variability) and, possibly, the chosen model structure. The first two can be partially compensated by increasing the observation period or observation frequency to better analyze the system dynamics.

For distributed models the variational estimation algorithm could be a natural choice, since it is scalable, i.e. it works efficiently for practically unlimited size of the control vector. That is why this method (branded as 4D-Var) is commonly used in meteorology and oceanography for operational forecasting and reanalysis (Ledimet and Talagrand, 1986; Rabier and Courtier, 1992). The method provides the exact mode of the posterior distribution by minimizing the cost-function defined over the given observation window. The key element of the method is the adjoint model which provides the precise gradient of the cost-function with respect to all elements of the control vector in a single run (Errico, 1997). This allows the fast converging gradient-based minimization methods to be used, such as the BFGS or the Newton-type. Quite often, the need for development of the adjoint model becomes an obstacle for practical implementation of this method. Heuristic methods such as the Nelder-Mead algorithm do not require the gradient to evaluate the descent directions, but converge slowly and are not suitable for solving problems in high dimensions. The same is true as for the general purpose statistical methods such as the Markov Chain Monte

Carlo (e.g. Metropolis-Hastings algorithm), so for the methods specially designed for hydrology applications, such as SUFI-2 (Abbaspour et al., 2007).

Let us consider the rainfall and potential evapotranspiration fields $P(x,t)$, $E(x,t)$, $\forall x \in \Omega$. We represent the hydrological model in Section 2.1 as an operator A mapping the input fields $P(x,t)$ and $E(x,t)$ into the discharge $Q_k(t)$ at the gauged nodes $x_k \in \Omega$, $k = 1, N_g$:

$$Q_k(t) = A(P(x,t'), E(x,t'), h(x,0), \theta(x), t), \forall x \in \Omega, \, t' \in (0,t), \tag{14}$$

where $h(x,t) = (h_p(x,t), h_t(x,t))^T$ is the state vector which includes the states of production and transfer reservoirs for all cells at time t, $\theta(x) = (c_p(x), c_t(x), v(x))^T$ is the parameter vector which includes the corresponding capacities and the routing velocities at all routing nodes, and N_g - the number of gauged routing nodes, i.e. where discharge observations are available. If the observation period is much longer than the characteristic time of the system (which is the case for calibration/re-analysis), one can use the trivial initial state $h(x,0) = 0$, but consider the observation window $t \in (t^*, T)$, where t^* is the relaxation period. Given the observed inputs $P^*(x,t')$, $E^*(x,t')$, $t' \in (0,t)$ and the output $Q_k^*(t)$, the calibration cost-function can be defined as follows:

$$J(\theta) = \sum_{k=1}^{N_g} a_k^{-1}(t^*) \int_{t=t^*}^{T} \left(A(P^*, E^*, 0, \theta, t) - Q_k^*(t) \right)^2 dt + \alpha \| B^{-1/2}(\theta - \theta^*) \|_{L^2}^2, \tag{15}$$

where B is the background error covariance, θ^* is a prior guess on θ, which comes from special measurements, land expertise or a modeling, α is the regularization parameter and a_k are the scaling constraints. If we consider

$$a_k(t^*) = \int_{t=t^*}^{T} \left(\langle Q_k^* \rangle - Q_k^*(t) \right)^2 dt,$$

where $\langle Q_k^* \rangle$ is the temporal mean of $Q_k^*(t)$, then for each k the misfit term becomes $1 - NSE$, where NSE stands for the Nash-Sutcliffe efficiency criterion (Nash and Sutcliffe, 1970) widely used in hydrology. In essence, (15) is more or less a standard quadratic cost-function similar to the one used in variational data assimilation (4D-Var), where the weight α is introduced to mitigate the uncertainty in θ^* and B. Let us note that this paper is focused on the parameter calibration problem involving long time series of observations.

We use additional constraints in the form

$$\theta_{min} \leq \theta \leq \theta_{max}, \tag{16}$$

where θ_{min} and θ_{max} are the bounds which come from the empirical knowledge or physical considerations. Thus, the optimal estimate of the parameters $\hat{\theta}$ is obtained from the condition

$$\hat{\theta} = \arg\min_{\theta} J(\theta), \tag{17}$$

given constraints (14) and (16).

Matrix B can be represented in the form $B = \sigma_\theta \cdot I\, C\, \sigma_\theta \cdot I$, where σ_θ is the vector of mean deviations of θ, C is the correlation matrix, I - the identity matrix, and '$\cdot$' stands for the element-wise (Hadamar) product. Next, the scaling of parameters is introduced, such that $\theta = \theta_{min} + \tilde{\theta}(\theta_{max} - \theta_{min})$, to ensure that $0 \leq \tilde{\theta} \leq 1$. Then, the penalty term in (15) takes the form

$$\alpha \|(\theta_{max} - \theta_{min}) \cdot \sigma_\theta^{-1} \cdot I\, C^{-1/2}(\tilde{\theta} - \tilde{\theta}^*)\|_{L^2}^2.$$

Assuming that $(\theta_{max} - \theta_{min}) \cdot \sigma_\theta^{-1} = const$, the cost-function (15) reads as follows:

$$J(\tilde{\theta}) = \sum_{k=1}^{N_g} a_k^{-1}(t^*) \int_{t=t^*}^{T} \left(A(P^*, E^*, 0, \theta) - Q_k^*\right)^2 dt + \alpha \|C^{-1/2}(\tilde{\theta} - \tilde{\theta}^*)\|_{L^2}^2, \tag{18}$$

given

$$\theta = \theta_{min} + \tilde{\theta}(\theta_{max} - \theta_{min}), \; 0 \leq \tilde{\theta} \leq 1. \tag{19}$$

The results presented in this paper correspond to the simplest approach to regularization: we assume that $C = I$, and the regularization parameter is chosen a-priori as a small value ($\alpha = 10^{-4}$) to insure the formal well-posedness of the calibration problem. More sophisticated approaches for regularization (non-trivial correlation matrix C and the optimal choice of α using the L-curve approach) have been utilized (Jay-Allemand et al., 2018), but not presented in this paper for the sake of simplicity. In practice, the simplifications mentioned above lead to a significantly more oscillating parameter fields, which does not seem to have a critical influence on the predictive performance of the model (in the open loop forecasting, at least).

Minimization of (18) given constraints (19) is performed by LBFGS-B (Limited memory Broyden-Fletcher-Goldfarb-Shanno Bound-constrained (Zhu et al., 1994)). The minimization process can be written in the form

$$\tilde{\theta}_{i+1} = \tilde{\theta}_i + \gamma H^{-1}(\theta_i) R[J'_{\hat{\theta}}(\theta_i)], \; i = 0, 1, \ldots, \; \tilde{\theta}_0 = \tilde{\theta}^*, \tag{20}$$

where $J'(\theta_i)$ and $H^{-1}(\theta_i)$ are the gradient (with respect to $\tilde{\theta}$) and the limited-memory inverse Hessian of (18) at point θ_i, respectively, γ is a descent step, i is the iteration number, and R is the gradient projection operator to account for the box constraints. Let us note that $H^{-1}(\theta_i)$ is directly computed inside the minimization algorithm in such a way that its norm is always bounded. This serves as an additional regularization, thus the solution $\hat{\theta}$ is always bounded, even for $\alpha = 0$ in (18), i.e. even without the penalty term. The gradient $J'(\theta_i)$ is obtained by solving the adjoint model. This model has been generated by the Automatic Differentiation engine Tapenade (Hascoet and Pascual, 2013), then manually optimized and, finally, verified using the standard gradient test.

The background value θ^* is used both as a starting point for iterations and in the penalty term. Given the fact that the information content of the test signal (rainfall) and observations (discharge) may not be sufficient to uniquely

identify the distributed coefficients, evaluating an appropriate θ^* becomes an important issue. Thus, the overall calibration process involves two steps. In the first step we consider a uniform approximation: $c_p(x) = \bar{c}_p$, $c_t(x) = \bar{c}_t$, $v(x) = \bar{v}$, $\forall x \in \Omega$. In this case (referred as '**uniform calibration**') the sought vector $\bar{\theta} = (\bar{c}_p, \bar{c}_t, \bar{v})^T$ consists of just three elements. For such low-dimensional problem, obtaining the globally optimal estimate $\hat{\bar{\theta}}$ (i.e. the one which

5   corresponds to the global minimum of (18)), is feasible by a variety of methods. In particular, we use a simple global minimization algorithm, the steepest descent method summarised in Edijatno (1991) In the second step we estimate the distributed parameters using the uniform estimate as a background, i.e. $\theta^* = \hat{\bar{\theta}}$. Here, three unknown parameters for each cell are estimated using the variational algorithm described above. This two step algorithm is referred as '**distributed calibration**'.

10   Parameter bounds are defined for each step. Numerical and physical considerations enforce the lower bounds, so that $(c_p, c_t, v) > 0$. For the uniform calibration, the upper bounds are chosen to preserve the model dynamics. For example, $5m/s$ is used as the velocity upper bound since above this value the flow delay does not decrease significantly. For the production and transfer reservoirs the upper bounds are set to $5000mm$ and $2000mm$, respectively, since the higher values do not noticeably change the model dynamics (reservoir states remain almost constant in

15   time). For the distributed calibration, bounds are re-computed as $\theta_{max} = b\hat{\bar{\theta}}$ and $\theta_{min} = \hat{\bar{\theta}}/b$. In particular, $b = 4$ is used for results presented in this paper. Further increasing b does not seem to have any influence on the estimates.

2.3   Study area and data

A French watershed, the Gardon d'Anduze, has been considered for testing our model and calibration algorithm.

20   Located in the western Mediterranean region, this catchment and its surrounding have been deeply studied in the framework of the HYMEX program (Drobinski et al., 2014) to understand the processes leading to flash floods. For instance, some studies exploited a number of very detailed field measurements during severe storm events (Braud et al., 2014; Vannier et al., 2014). Others tested hypothesis using physically distributed models, for instance the MARINE model (Roux et al., 2011; Garambois et al., 2013, 2015; Douinot et al., 2016, 2018) or the VCN-p model

25   (Braud et al., 2010; Vannier et al., 2016). A few conceptual distributed models were also considered in this area, such as those implemented into the ATHYS platform (Bouvier and DelClaux, 1996; Laganier et al., 2014; Tramblay et al., 2010).

The main properties of the Gardon d'Anduze are described in Darras (2015). In brief, this is a steep mountainous

30   watershed with a dense hydrographic network spreading over $540\ km^2$ in the East part of the Cévennes mountain (France). The difference in levels between the highest elevation point and Anduze is about 800 meters and the slope reaches 50% in the upstream part. Metamorphic (schist) but fractured geological formation dominates the watershed. Water infiltrates very quickly (the saturated hydraulic conductivity is greater than $100\ mm.h^{-1}$). The water circulation appends mainly underground, but with very short response times (less than 12-h). This area is
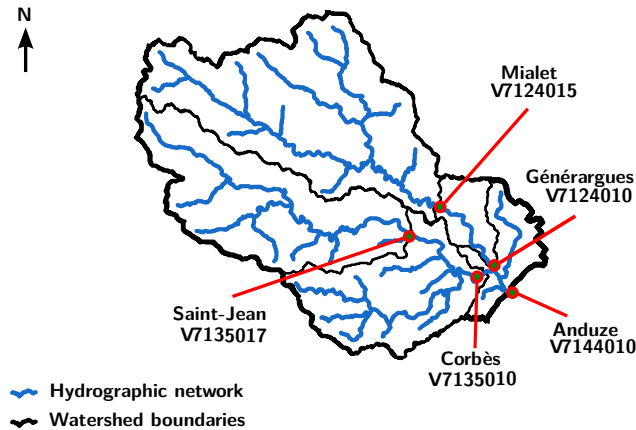
Figure 2. The Gardon watershed at Anduze: hydrographic network (blue) and gauging stations V7124015, V7124010, V7135017, V7135010, V7144010 (red).

governed by a transitional Mediterranean-Oceanic climate with warm and dry summers, alleviated by the oceanic influence, followed by recurrent short, intense but persistent heavy rainfalls in autumn and winter, known as "épisode méditerranéen", generating flash floods.

5   This watershed is well gauged: at least five stations with continuous data collection are operational here (see Fig.2 and Tab.1). For numerical experiments, the discharge data have been extracted from the HYDRO database of the French ministry in charge of environment. Rainfall gridded data has been provided by Météo-France. It is is a pseudo-real time reanalysis (ANTILOPE J+1, i.e. available one day after the current date), merging radar rainfall estimation with in-situ rain gauges. The gridded potential evapotranspiration is computed using inter-annual air

10 temperature values and the formula developed by Oudin et al. (2005). The temperature data was provided by the SAFRAN reanalysis (Vidal et al., 2010). All the time series have been processed at an hourly time step, over the continuous 2007-2018 period. All the gridded data is defined at a $1\,km \times 1\,km$ spatial resolution, over the same $46\,km \times 40\,km$ domain overlapping the watershed. Furthermore, the flow direction (8 directions) map and the flow accumulation map have been carefully checked, in order to ensure that every cell is connected to the correct down-

15 stream cell.

2.4   Investigating methodology

The variational algorithm described in Sect. 2.2 is applied to the hydrological model presented in Sect. 2.1, using the Gardon d'Anduze watershed as a benchmark. The number of 'active' cells (i.e. included into the watershed) is

Table 1. Characteristics of the five gauging stations on the Gardon watershed. QIX2 and QIX10 stand for the quantiles discharge, respectively two and ten years return period.

Rivers and station names	Codes	Surfaces (km^2)	QIX2 (m^3/s)	QIX10 (m^3/s)
The Gardon de Mialet at Mialet	V7124015	219	243	486
The Gardon de Mialet at Générargues	V7124010	244	346	618
The Gardon de Saint-Jean at Saint-Jean-du-Gard	V7135017	158	230	460
The Gardon de Saint-Jean at Saint-Jean de Corbès	V7135010	262	320	598
The Gardon d'Anduze at Anduze	V7144010	543	634	1300

540, so the total number of parameters to be calibrated is 3×540.

The calibrated model validation step consists in checking the model predictive performance (referred as MPP onwards) using the data not involved in calibration. That is, the full set of observations $Q_k^*(t)$, $k = 1, \ldots, N_g$, $t \in (0, T)$ is divided in two complementary subsets: calibration subset and validation subset. Since Q^* depends on k (defines the spatial distribution of sensors) and t, we distinguish the temporal, spatial, and spatio-temporal validation, following the split sample test defined by Klemes (1986). In particular, we divide the whole period in two parts: $P1$ - from 01/01/2008 to 01/01/2013 and $P2$ - from 01/01/2013 to 01/01/2018. Each period $P1$ and $P2$ can be considered as calibration or validation period. A model warm-up of one year long is performed before starting the simulations. We assume that one year is enough, according to recommendations by Perrin et al. (2003).

If data from a station is used in calibration, the corresponding catchment is called the "calibration catchment", otherwise it is call the "validation catchment".

Both the calibration quality and the MPP in validation are measured using the NSE criterion and the Kling–Gupta efficiency (KGE) criterion (Gupta et al., 2009).

The spatio-temporal measured discharge data is partitioned into calibration and validation complementary sets. Then, we refer to:

a) "**temporal validation**" - if MPP is evaluated for all calibration catchments over the validation period;

b) "**spatial validation**" - for all validation catchments over the calibration period;

c) "**spatio-temporal validation**" - for all validation catchments over the validation period.

The following numerical experiments have been performed:

1. **calibration uniform-5-sta / calibration distributed-5-sta** - uniform and distributed calibration, respectively, using discharge data from all five gauging stations, calibration periods $P1$ or $P2$. This is followed by temporal

Table 2. Selection of major floods for each period P1 and P2 at station Anduze (V7144010)

Events names	Date	Maximum peak discharge
EVE1/P1	2008/10/21 - 2008/10/23	1020 m^3/s
EVE2/P1	2008/10/31 - 2008/11/07	1030 m^3/s
EVE3/P1	2009/01/31 - 2009/02/05	390 m^3/s
EVE4/P1	2011/10/31 - 2011/11/08	1070 m^3/s
EVE1/P2	2014/09/17 - 2014/09/21	1080 m^3/s
EVE2/P2	2014/10/09 - 2014/10/16	1180 m^3/s
EVE3/P2	2015/09/12 - 2015/09/15	1120 m^3/s
EVE4/P2	2015/10/27 - 2015/10/29	1530 m^3/s

validation, i.e. the parameter estimate obtained using data from $P1$ is validated on data from $P2$, and vice versa. The appends **uniform-5-sta** and **distributed-5-sta** to the 'temporal validation' in Fig.3 indicate the relevant calibration procedure.

2. **calibration uniform-1-sta** / **calibration distributed-1-sta** - uniform and distributed calibration, respectively,
5 using discharge data from one downstream gauging station (Anduze), calibration periods $P1$ or $P2$. This is followed by spatial validation using data from remaining four gauging stations (Générargues, Mialet, Saint-Jean and Corbès), calibration periods $P1$ or $P2$, and by spatio-temporal validation on data from remaining four gauging stations, but for validation periods $P2$ or $P1$.

3. **ensemble distributed-1-sta** - multiple distributed calibration using discharge data from the Anduze gauging
10 station, starting from different uniform priors.

The main purpose of experiments 1 and 2 is to quantify the anticipated MPP improvement, achieved in "distributed calibration". Given the rainfall data, we compare the ability of the calibrated model to predict the discharge at observation points without using the discharge data for the validation period (exp.1, temporal validation); then the ability to resolve the spatial distribution of discharge in ungauged areas, given the discharge data for the validation
15 period at the catchment outlet (exp.2, spatial validation), and the ability to predict the discharge in ungauged areas and without using the discharge data for the validation period (exp.2, spatio-temporal validation). Clearly, the latter is the ultimate performance test. The purpose of experiment 3 is to investigate the stability of the parameter estimates with respect to their priors. This is necessary to assess the impacts of equifinality and limitations related to the local-search minimization.

20 In addition, the current MPP is analyzed for the eight major flood events for periods $P1$ and $P2$, listed in Tab.2. Three others criteria from (Artigue et al., 2012) are used, which compare the magnitude and the synchronization of the modeled and observed flood peak:

1. The Percentage Peak Discharge P_D:

$$P_D = 100 \times \frac{Q_{max}}{Q^*_{max}}, \tag{21}$$

where $Q_{max} = Q(t_m)$ and $Q^*_{max} = Q^*(t^*_m)$ are the predicted and the observed maximum discharges, respectively. These maximum values are achieved at different time instants t_m and t^*_m, within the chosen time period;

2. The Synchronous Percentage of the Peak Discharge S_{PPD}:

$$S_{PPD} = 100 \times \frac{Q(t^*_m)}{Q^*_{max}}; \tag{22}$$

3. The Peak delay P_D:

$$P_d = t_m - t^*_m. \tag{23}$$

3 Results

3.1 Performance analysis

The results associated with experiments 1 and 2 are presented in Fig.3 in a "statistical" form (as a distribution of the NSE criterion ranked in increasing order), without relation to the period or gauge station.

Fig.3 (upper/left), shows the results of "uniform" and "distributed" calibration from exp.1. All five gauging stations are involved in calibration over 2 periods, thus we have 5×2 calibration points. One can see that the distributed calibration allows a much better approximation of the observed discharge than the uniform one. This result confirms that the data assimilation procedure works. It also suggests that hydrological properties of the catchment are not uniform and may be captured using distributed parameters. On the other hand, the mismatch between the predicted and observed discharges remains significant. Since the model looks over-parametrized and the regularization parameter in (18) is very small, this indicates that a few issues, either alone or in combination, may be presented: corrupted data (the data used is not a synthetic one), deficient model structure (such as unaccounted sink term, for example), a local minimum is reached instead of the global one. Some of these issues will be later discussed. Fig.3 (upper/right), shows the same results for exp.1., but this time in temporal validation. One can see that the distributed calibration allows to achieve a better "global" temporal MPP than the uniform one.

Fig.3 (lower/left), shows the results of spatial validation of exp.2 (i.e. calibrating only with data from the Anduze gauging station). The remaining four gauging stations are involved in validation for two time periods, thus we have 4×2 spatial validation points. The calibration results for the Anduze station are not presented graphically, but the NSE values achieved are as follows (for P1/P2 respectively): uniform 0.82/0.78, distributed 0.93/0.88, whereas the KGE values are: uniform 0.81/0.71, distributed 0.89/0.69. One can see once again that the distributed calibration allows clearly to achieve a better global spatial MPP than the uniform one. Finally, Fig.3 (lower/right) shows
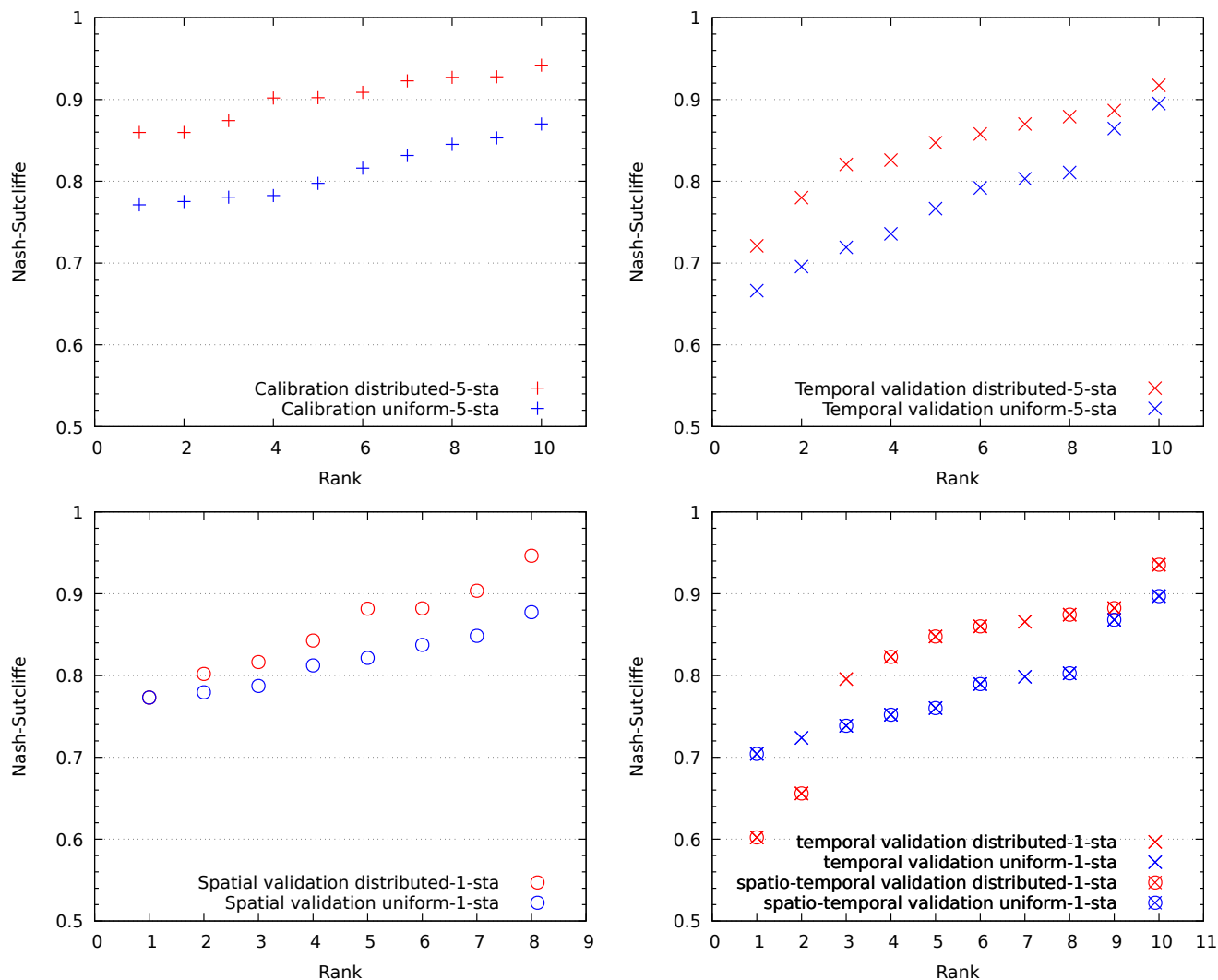
Figure 3. 'Statistical' distribution of the NSE criterion comparing distributed versus uniform calibration and the corresponding validation results: calibration of exp.1 - upper/left, temporal validation of exp.1 - upper/right, spatial validation of exp.2 - lower/left, and spatio-temporal validation exp.2 - lower/right.

the results of spatio-temporal validation (exp.2), evaluated over the period not used for calibration. As before, only data from the Anduze gauging station is used for calibration, but data from all five gauging stations from a different time period is used for validation, giving 5×2 validation points. Two of them (in "×") show the corresponding temporal validation results at the Anduze gauge station, others (shown in "⊗") - the spatio-temporal validation results at the remaining gauge stations. One can see that the spatio-temporal MPP is generally better if the distributed

calibration is used.

3.2 Period-based analysis

To get a more detailed view on the results of exp 2., Fig.4 relates each NSE value to the particular time period and
gauging station. Here, the upper/left panel presents the NSE values calculated over the period $P1$, with parameters
optimized over the same period (calibration); the upper/right panel presents the NSE values calculated over $P1$,
with parameters optimized over $P2$ (validation). Conversely, the lower/left panel presents the NSE values calcu-
lated over the period $P2$, with parameters optimized over the same period; the lower/right panel presents the values
calculated over $P2$, with parameters optimized over $P1$. All panels presents results for the uniform and distributed
parameters (blue and red respectively). The similar figure has been obtained for exp. 1, but not presented here since
the results are also similar. Based on this figure the following observations can be made:

1. Considering the results obtained with uniform paramters (blue), the NSE values are always better (larger) when
calculated over the period $P1$, whatever case is considered: calibration (+), spatial validation (o), temporal valida-
tion ($\times$) or spatio-temporal validation ($\otimes$).

2. Considering the results obtained with distributed parameters (red), better results are always obtained when the
NSE values are calculated over $P1$ in calibration (+) and temporal validation ($\times$). But in spatial validation (o), bet-
ter results are obtained on $P2$, for two out of four upstream stations: Mialet and Corbes (V7124015 and V7135010,
respectively).

3. Comparing the NSE values for the uniform (blue) and the distributed (red) calibration, we notice that for the
latter we obtain better results, except in two cases: in spatial validation over $P1$ for Mialet and Corbes (V7124015
and V7135010), and in spatio-temporal validation over $P2$ for Corbes and Saint-Jean (V7135010 and V7135017).
Note that in both cases the distributed parameters have been calibrated over $P1$.

To complete the analysis, the MPP obtained in spatio-temporal validation at Mialet (V7124015) and Saint-Jean
(V7135017) - two stations identified as 'particular' just above - have been studied in more detail, for 2×4 flood
events described in Tab.2, corresponding to the four biggest flood over each period. The corresponding hydrographs
are plotted in Fig.5, and the resulting MPP criteria NSE, KGE, PPD, S_{PPD} and P_D are presented in Tab.3 and
Tab.4. Based on these results the following conclusions can be made:

1. Flood events at those stations which occur during the period P1 are well simulated using both uniform and
distributed set of parameters calibrated over $P2$ ($\overline{NSE} > 0.70$ and $\overline{KGE} > 0.60$). In particular, the prediction of
the event $3/P1$ is noticeably improved for the distributed calibration. The simulated flood peak is well synchronized
with the observed one, though slightly shifted when the distributed calibration is used. Note that these minor shifts
are not critical for the peak discharge prediction as PPD and S_{PDD} remain similar;
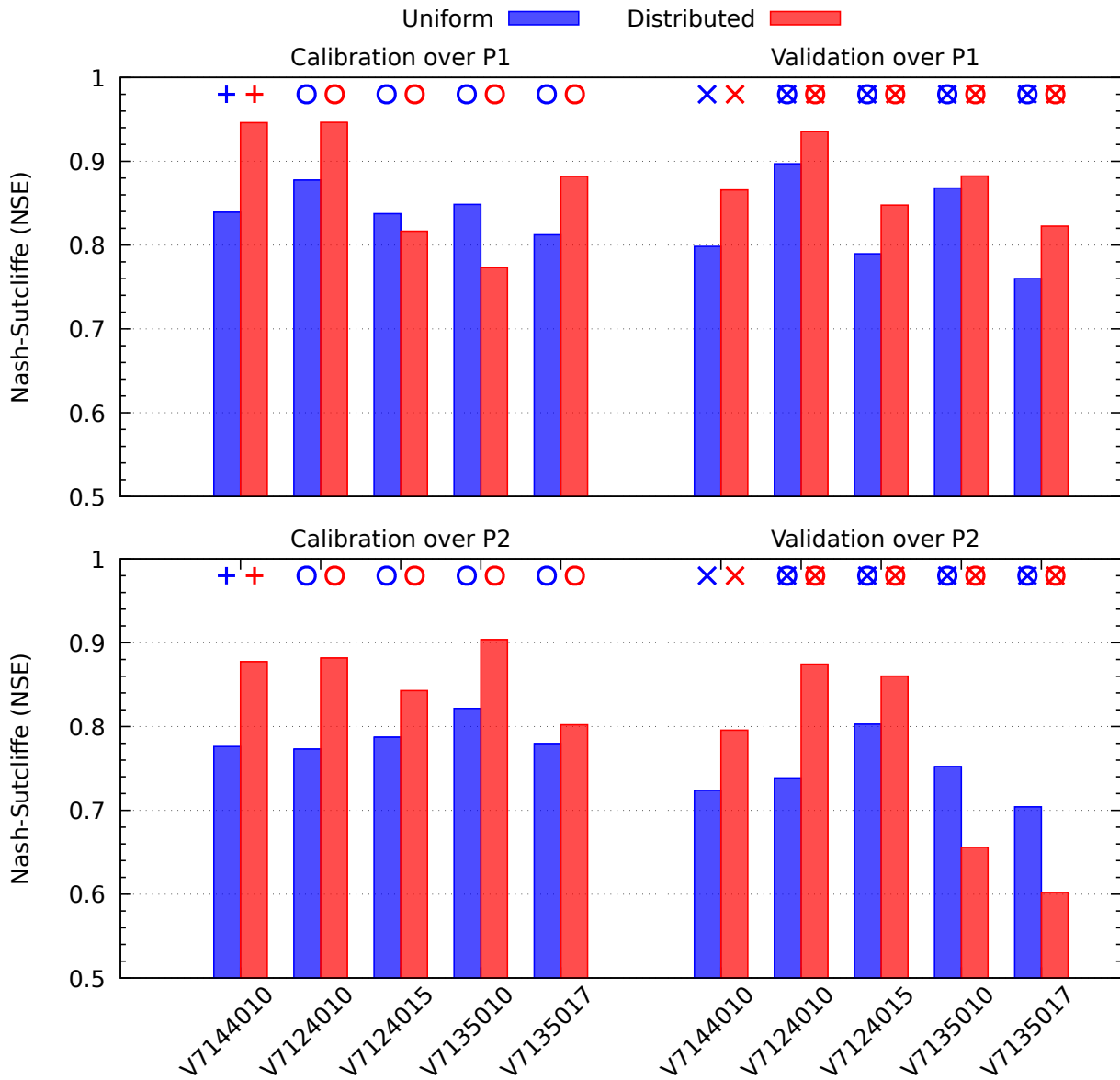
Figure 4. *NSE* criterion calibration and corresponding validation results for exp.2 (one upstream gauging station), by stations and periods (*P*1 upper, *P*2 lower, for uniform paramters (blue) and distributed parameters (red).

Table 3. MPP criteria (NSE, KGE, S_{PPD}, P_d) computed for major flood events selected over the period $P1$, using distributed (**dist**) and uniform (**unif**) calibration over $P2$.

		NSE		KGE		PPD		S_{PPD}		P_D (hours)	
		dist	unif	dist	unif	dist	unif	dist	unif	dist	unif
EVE1/P1	V7124015	.38	.64	.36	.47	47.00	54.72	40.15	54.72	1	0
EVE1/P1	V7135017	.71	.64	.84	.59	80.69	121.23	77.15	121.23	1	0
EVE2/P1	V7124015	.95	.93	.90	.91	92.33	87.73	92.33	87.73	0	0
EVE2/P1	V7135017	.79	.87	.68	.84	66.26	79.28	64.43	79.28	-1	0
EVE3/P1	V7124015	.92	.68	.91	.57	102.38	126.21	100.43	126.21	-1	0
EVE3/P1	V7135017	.76	.20	.57	.18	119.18	141.48	115.08	134.26	-2	-3
EVE4/P1	V7124015	.93	.92	.82	.81	94.62	120.92	94.62	120.92	0	0
EVE4/P1	V7135017	.71	.86	.47	.63	90.10	100.70	87.82	100.70	1	0
Average		0.77	0.72	0.69	0.63	86.57	104.03	84.00	103.13	-0.13	-0.38

2. In contrast, the prediction of flood events which occur during $P2$ is unsatisfactory. Moreover, the results are even worse for distributed calibration. Modeled flood peaks are severely under-estimated at station Saint-Jean (V7135017) for all four events, both for uniform and distributed calibration. At station Mialet (V7124015) the peak discharge is over-estimated for the distributed calibration.

These results are consistent with those from Fig.4 in spatio-temporal validation ($\otimes$), for the same two stations. A smaller cost achieved during calibration does not necessary imply a better MPP, indicating an excessive assimilation of errors associated to $P1$.

10 Fig.6 and Fig.7 represent the maps of the calibrated parameters obtained in exp.1 and exp. 2, respectively, whereas Tab.5 provides the corresponding uniform values $\hat{\bar{\theta}}$ used as priors in the variational estimation step. Comparing the left and right panels in Fig.7 corresponding to different time periods $P1$ and $P2$ one can notice a significant difference between the calibrated capacities c_p and c_t. The spatial variability of c_p and c_t is also higher when the calibration is performed on period $P1$. One can notice that the results of the uniform calibration are also different

15 for both periods. Concerning the routing velocity v, the maps look rather similar. The velocity changes occur mainly at the cells located in the drainage (see Fig.2), because the sensitivity of the cost function w.r.t. the velocities in these cells is the largest. The trend is that these velocities increase during calibration. Note that the velocities above

Table 4. MPP criteria (NSE, KGE, S_{PPD}, P_d) computed for major flood events selected over the period $P2$, using distributed (**dist**) and uniform (**unif**) calibration over $P1$.

		NSE		KGE		PPD		S_{PPD}		P_D (hours)	
		dist	unif	dist	unif	dist	unif	dist	unif	dist	unif
EVE1/P2	V7124015	.43	.45	.72	.64	105.32	86.69	17.00	30.70	31	32
EVE1/P2	V7135017	-.10	.24	-.12	.22	9.69	16.27	5.14	14.15	31	2
EVE2/P2	V7124015	.43	.86	.51	.90	148.00	73.79	126.57	73.79	-1	0
EVE2/P2	V7135017	.31	.47	.13	.37	18.76	29.48	17.86	17.51	39	40
EVE3/P2	V7124015	.59	.63	.41	.34	124.36	98.42	123.30	91.35	-1	4
EVE3/P2	V7135017	.27	.35	.09	.27	14.96	22.68	13.08	13.33	5	6
EVE4/P2	V7124015	.94	.79	.83	.73	85.69	58.20	85.69	58.20	0	0
EVE4/P2	V7135017	.26	.46	.02	.24	21.64	32.94	21.64	31.17	0	1
Average		0.39	0.53	0.32	0.46	66.05	52.31	51.29	41.28	13	10.625

Table 5. Optimal uniform set of parameters for experiments uniform-5-sta / uniform-1-sta.

Parameters	Period P1 (5-sta/1-sta)	Period P2 (5-sta/1-sta)
c_p (mm)	1014.2 / 1276.5	1288.5 / 1202.3
c_t (mm)	250 / 214.7	150.7 / 150.1
v (m/s)	5 / 5	5 / 5

5 m/s does not affect significantly the delay between cells. Moreover, the routing velocities obtained are generally consistent with the fast hydrological response of the Gardon watershed (Darras, 2015). A few questions concerning the results in Fig.6 and Fig.7 should be answered. For example, why are the estimates associated to periods $P1$ and $P2$ so different? Is it an 'algorithmic' issue (for example, due to the use of the local-search minimization, uncorrelated priors, etc.) which can be resolved by improving the calibration algorithm, or a 'fundamental' issue related to identifiability (which depends of the data available, properties of the model under investigation, and its adequacy to the real natural system and its physical characteristics)?We try to answer this question in the next section.

3.3 Stability analysis

An inverse problem is well-posed if a solution to the problem exists, is unique, and is continuous with respect to the input data. Let us consider a mathematical model describing a certain physical phenomenon and assume that some variables of this phenomenon are partly observed. If the model is perfect (adequate) and observations are exact then, given the input, the model's output has to match observations. This implies that the minimum of a cost-function penalizing the mismatch (mismatch functional) equals to zero. Parameter calibration problems are often ill-posed in terms of the uniqueness (equifinality): there may exist a set of solutions for which the mismatch functional equals to zero. However, the 'true' value of parameters does exist as one element of this set. If the model involved is nonlinear with respect to its parameters, the mismatch functional may contain additional minimum points where its value is not zero. While the corresponding parameters do not belong to the set of solutions, in the local-search minimization methods such points are interpreted as solutions. Adding a penalty (regularization) term to the mismatch functional allows one particular solution, which is the 'closest' to the prior in terms of a chosen norm, to be defined. This makes the problem formally well-posed but, in practical terms, transforms the non-uniqueness issue into the issue of choosing the prior. Thus, investigating the stability of the estimates with respect to the priors is an important step in design and validation of a calibration algorithm. In particular, such analysis allows the parts of the solution dominated by observations and by the prior to be distinguished.

A straightforward approach implies solving an ensemble of calibration problems involving random (or quasi-random) uniform priors subjected to box constraints (16). Let us remind that the priors are used in two ways: as starting points for minimization, and to define the penalty term. The influence of the latter has been neglected by choosing small α in (18). Let $\hat{\theta}|_{\bar{\theta}_l}$ be the parameter estimate conditioned on the uniform prior $\bar{\theta}_l$, $l = 1, \ldots, L$ from the ensemble of priors of size L. Then, the stability for each element of the parameter vector is measured by the 'standard deviation' given as follows:

$$\sigma_\theta = sign(a)\sqrt{|\,a\,|}, \quad a = \frac{1}{L}\sum_{l=1}^{L}\left[(\hat{\theta}|_{\bar{\theta}_l} - \langle\hat{\theta}\rangle)^2 - (\bar{\theta}_l - \langle\bar{\theta}\rangle)^2\right], \tag{24}$$

where $\langle\bar{\theta}\rangle$ and $\langle\hat{\theta}\rangle$ are the ensemble average of priors and estimates, respectively. One can see that the negative values of σ_θ correspond to the case when the solution tends to approach the same value for all priors, i.e. it is dominated (or stabilized) by observations, whereas the positive values of σ_θ - to the case when the solution is dominated by the prior.

In reality, the conceptual GRD model used in this study is a fairly crude approximation of the hydrological phenomenon. Thus, no solution can be considered as a 'truth', but as an interpretation of data, given the model and the judgment criteria (cost-function). Moreover, the measured data (test signal and observations) are not perfect. These imperfections result into a 'generalized observation error'. The stability analysis described above can also be applied in this case, though understanding of results is more difficult. For example, the ensemble average of the mismatch functional values (achieved in minimization) can be considered as a reference level. The parameter estimates which

Table 6. Initial and final values of the cost-function (18) for different uniform priors for periods $P1$ (upper table) and $P2$ (lower table), exp.3.

		1 $\bar{c}_p = 425.5$	2 $\bar{c}_p = 851.0$	3 $\bar{c}_p = 1276.5$	4 $\bar{c}_p = 1702.0$
1	$\bar{c}_t = 71.5$	1.20/0.054	0.689/0.054	0.528/0.057	0.451/0.057
2	$\bar{c}_t = 143.1$	0.563/0.055	0.280/0.056	0.210/0.057	0.195/0.058
3	$\bar{c}_t = 214.7$	0.350/0.057	0.186/0.053	0.161/0.054	0.177/0.054
4	$\bar{c}_t = 286.2$	0.280/0.057	0.185/0.055	0.185/0.056	0.217/0.052

		1 $\bar{c}_p = 413.0$	2 $\bar{c}_p = 825.9$	3 $\bar{c}_p = 1238.9$	4 $\bar{c}_p = 1651.9$
1	$\bar{c}_t = 50.0$	1.39/0.130	0.924/0.130	0.776/0.131	0.707/0.130
2	$\bar{c}_t = 100.1$	0.642/0.125	0.369/0.126	0.296/0.132	0.288/0.125
3	$\bar{c}_t = 150.1$	0.396/0.134	0.252/0.124	0.224/0.130	0.24/0.129
4	$\bar{c}_t = 200.1$	0.325/0.131	0.26/0.121	0.258/0.136	0.286/0.126

correspond to the values around this level can be considered as possible solutions, whereas the outliers must be discarded.

The stability analysis (exp.3) has been performed for $L = 16$ configurations of uniform priors $\bar{c}_p$ and $\bar{c}_t$, see Tab.6, with the same routing velocity $\bar{v} = 5$ m/s. The Table shows the values of the cost-function $J(\theta)$ (18) for θ before and after minimization.

One can see that all minimization processes for a chosen assimilation period converge to a similar value of the cost-function: for $P1$ the mean value is 0.055 and the standard deviation is 0.002, i.e. about 3.6% of the mean, for $P2$ - the corresponding numbers are 0.129, 0.004 and 3.1%. No obvious outliers have been observed, which indicates that the cost-function surface is sufficiently regular and the issue of 'local-search against global-search' is not critical. The latter is not surprising since, considering the operators involved, the model seems to be mildly nonlinear.

The spatial distributions of σ_θ are presented in Fig.8, where the stable areas of the estimated parameter fields, i.e. those influenced by observations, are shown in blue. The purpose of this analysis is to understand why the estimates associated to periods $P1$ and $P2$ are so different. In particular, the question rises concerning the high capacities obtained for $P1$, see red areas in Fig.7(left) for c_p and dark-yellow areas for c_t. In contrast, the capacities obtained for $P2$ are the lowest in the corresponding areas. However, comparing Fig.7 and Fig.8 we notice that these 'questionable' areas in Fig.7 largely coincide with the blue (stable) areas in Fig.8. This clearly indicates that the corresponding

estimates are determined by the observed data used in each case. Thus, one may suspect here the data information content issue, and/or the data interpretation criteria (cost-function) issue, and/or the model adequacy issue, rather than algorithmic issues. This is the main conclusion drawn from the stability analysis. One can also notice that the estimates associated to $P2$ (right) are generally more stable than those associated to $P1$ (left), whereas the ensemble average cost-function value achieved for $P2$ is larger than for $P1$, i.e. 0.129 against 0.055. While a better minimization result has been achieved for $P1$, it looks like more error have been assimilated in this case.

4   Discussion and Conclusions

The validation results presented in Sec. 3.1 and 3.2 confirm that the distributed calibration globally improves the temporal and spatial MPP (measured by NSE) as compared to the uniform calibration. The conclusions are less definite with the spatio-temporal MPP, but this is the most difficult performance test. Moreover, the global improvement does not mean that any particular event could be better predicted, as follows from Sec.3.2. We observe that, on one hand, the capacity c_p and c_t estimates obtained using different calibration periods are quite different; on the other hand, for a chosen calibration period these estimates are relatively stable with respect to their priors. The latter means that the difference is rather due to a different data involved in calibration, than due to the algorithmic or identifiability problems, see Sect.3.3. Let us note that the cross-validation experiments could help the best set of parameters to be selected. For example, the MPP analysis above suggests that the sets calibrated using data from $P2$ should be preferred.

It seems that the routing velocity v is the most stable among all estimated parameters: the velocity fields plotted in Fig.6 and Fig.7 remain similar for different experiments. Looking at the hydrographic network in Fig.2, one can see that the velocities are generally much higher along the main drains than on the side slopes, which is in agreement with the true physical behavior of the system, though the routing scheme applied is conceptual. One can notice a few occasions where the velocities are lower in the drain: the Gardon de Saint-Jean, exp.1($P2$), the south-west tributary connected to Corbès, exp.1($P1$), and the upstream Gardon catchment in exp.2($P2$). This is likely to be a consequence of an overestimated uniform background, $\bar{v} = 5$ m/s.

Calibration of the distributed hydrological models is a difficult task, with the data information content issue, the data interpretation criteria issue, and the model adequacy. Some of this issues will be addressed in the nearest future. For example, the use of the Gaussian likelihood which leads to the quadratic cost-function of the type (15) does not seems to be the best choice. Taking into account that the discharge itself is a positive variable and the discharge observation error is, most likely, an increasing function of discharge, using the gamma likelihood looks more appropriate.

It is evident that, because of its conceptual nature and simplicity, the GRD model has some structural limitations. Looking for a simple structural upgrade, which may help to improve the adequacy without increasing noticeably the dimensions and computational costs, is an important future task. Another one is to provide better priors. For instance, one can use the non-uniform priors. In particular, for the capacities c_p and c_t one could consider locally uniform values relevant to the given hydro-geological or soil occupation class. For the velocity, a higher value in the drainage network with respect to the accumulated flow surface have to be enforced. The mentioned above subjects will be addressed in the immediate future research.

In this paper, the model has been calibrated using data from different time periods and the cross-validation experiments have helped to select the best optimal set of the distributed parameters. However, using a longer calibration period may not necessarily improve the model predictive performance due to the likely presence of very different hydrological regimes over the extended period, including some extreme cases. As a way forward, one could consider calibrating the model independently for different hydrological regimes. This approach is coherent to the idea of the "pooled analysis". Dependent on the calibration strategy, different parameter sets could be used for the prediction purpose. In the operational flood forecasting context, the model parameters are likely to be fixed, whereas the real-time update of the model initial state should be considered instead. In that case, the initial states of the distributed reservoirs will serve as a control vector and the assimilation will be performed over a relatively short assimilation window (comparable to the characteristic time of the system). Finally, running ensemble of models with different calibrated sets of parameters could be considered. In the framework of a flash-flood warning system design, the latter approach could be combined with an automatic predictive control strategy such as the tree-based-model (Ficchì et al., 2016).

In summary, the variational approach based on the adjoint model has proved its great computational efficiency and relevance for solving the calibration problem involving the distributed hydrological model GRD. Technically, this problem can be solved over long time periods and for large spatial areas. The difficulties discovered in this process are the fundamental issues of calibration, not related to the chosen method. The answer to the main research question formulated at the beginning of this paper is positive: it is possible and beneficial to calibrate and, then, use distributed parameters, rather than uniform parameters. Variationnal algorithm involving adjoint sensitivities has proved to be an efficient tool for such calibration. The calibration quality is expected to be improved by using a more appropriate cost-function and by enhancing the model structure. Overall, this means that the suggested research and hydrological forecasting tool development direction is quite promising.

Competing interests. The authors declare that there are no competing interests.

Acknowledgements. This research has been funded by the French "Agence Nationale pour la recherche" (ANR) as a PhD, in the framework of the PICS project "Prévision immédiate intégrée des impacts des crues soudaines". It also contributes to the 2010-2020 HyMeX (Hydrological Cycle in the Mediterranean Experiment) program. Authors wish to thank Etienne Leblois (INRAE-Lyon) for having provided the flow direction map used in this study. Meteorological and hydrological data was provided by Meteo-France and SCHAPI respectively. The three anonymous referees are also thanked for their constructive comments and suggestions.

References

Abbaris, A., Dakhlaoui, H., Thiria, S., and Bargaoui, Z.: Variational data assimilation with the YAO platform for hydrological forecasting, Proceedings of the International Association of Hydrological Sciences, Volume 364, 2014, pp.3-8, 364, 3–8, https://doi.org/10.5194/piahs-364-3-2014, 2014.

5 Abbaspour, K. C., Yang, J., Maximov, I., Siber, R., Bogner, K., Mieleitner, J., Zobrist, J., and Srinivasan, R.: Modelling hydrology and water quality in the pre-alpine/alpine Thur watershed using SWAT, Journal of Hydrology, 333, 413–430, 2007.

Anderson, R. M., Koren, V. I., and Reed, S. M.: Using SSURGO data to improve Sacramento Model a priori parameter estimates, Journal of Hydrology, 320, 103–116, https://doi.org/10.1016/j.jhydrol.2005.07.020, publisher: Elsevier, 2006.

10 Arnaud, P., Lavabre, J., Fouchier, C., Diss, S., and Javelle, P.: Sensitivity of hydrological models to uncertainty in rainfall input, Hydrological Sciences Journal–Journal des Sciences Hydrologiques, 56, 397–410, 2011.

Artigue, G., Johannet, A., Borrell, V., and Pistre, S.: Flash flood forecasting in poorly gauged basins using neural networks: case study of the Gardon de Mialet basin (southern France), 2012.

Bell, V. A., Kay, A. L., Jones, R. G., and Moore, R. J.: Development of a high resolution grid-based river flow model

15 for use with regional climate model output, Hydrology and Earth System Sciences Discussions, 11, 532–549, https://hal. archives-ouvertes.fr/hal-00305636, 2007.

Beven, K.: Changing ideas in hydrology - The case of physically-based models, Journal of Hydrology, 105, 157–172, https://doi.org/10.1016/0022-1694(89)90101-7, 1989.

Beven, K.: Prophecy, reality and uncertainty in distributed hydrological modelling, Advances in Water Resources, 16, 41–51,

20 1993.

Beven, K.: How far can we go in distributed hydrological modelling?, Hydrology and Earth System Sciences, 5, 1–12, https://doi.org/10.5194/hess-5-1-2001, 2001.

Borga, M., Anagnostou, E. N., Blöschl, G., and Creutin, J. D.: Flash flood forecasting, warning and risk management: the HYDRATE project, Environmental Science & Policy, 14, 834–844, https://doi.org/10.1016/j.envsci.2011.05.017, 2011.

25 Bouvier, C. and DelClaux, F.: ATHYS: a hydrological environment for spatial modelling and coupling with GIS, IAHS Publications-Series of Proceedings and Reports-Intern Assoc Hydrological Sciences, 235, 19–28, 1996.

Braud, I., Roux, H., Anquetin, S., Maubourguet, M.-M., Manus, C., Viallet, P., and Dartus, D.: The use of distributed hydrological models for the Gard 2002 flash flood event: Analysis of associated hydrological processes, Journal of Hydrology, 394, 162–181, https://doi.org/10.1016/j.jhydrol.2010.03.033, 2010.

30 Braud, I., Ayral, P. A., Bouvier, C., Branger, F., Delrieu, G., Le Coz, J., Nord, G., Vandervaere, J. P., Anquetin, S., Adamovic, M., Andrieu, J., Batiot, C., Boudevillain, B., Brunet, P., Carreau, J., Confoland, A., Didon-Lescot, J. F., Domergue, J. M., Douvinet, J., Dramais, G., Freydier, R., Gérard, S., Huza, J., Leblois, E., Le Bourgeois, O., Le Boursicaud, R., Marchand, P., Martin, P., Nottale, L., Patris, N., Renard, B., Seidel, J. L., Taupin, J. D., Vannier, O., Vincendon, B., and Wijbrans, A.: Multi-scale hydrometeorological observation and modelling for flash flood understanding, Hydrology and

35 Earth System Sciences, 18, 3733–3761, https://doi.org/10.5194/hess-18-3733-2014, https://www.hydrol-earth-syst-sci.net/ 18/3733/2014/, 2014.

Braud, I., Borga, M., Gourley, J., Hurlimann Ziegler, M., Zappa, M., and Gallart, F.: Flash floods, hydro-geomorphic response and risk management, Journal of hydrology, 541, 1–5, 2016.

Castaings, W., Dartus, D., Le Dimet, F. X., and Saulnier, G. M.: Sensitivity analysis and parameter estimation for distributed hydrological modeling: potential of variational methods, Hydrology and Earth System Sciences, 13, 503–517, https://doi.org/10.5194/hess-13-503-2009, 2009.

Collier, C.: Flash flood forecasting: What are the limits of predictability?, Quarterly Journal of the Royal Meteorological Society, 133, 3–23, https://doi.org/10.1002/qj.29, 2007.

Darras, T.: Flash flood forecasting by statistical learning, Ph.D. thesis, Université Montpellier, https://tel.archives-ouvertes.fr/tel-01816929, 2015.

De Lavenne, A., Andréassian, V., Thirel, G., Ramos, M.-H., and Perrin, C.: A Regularization Approach to Improve the Sequential Calibration of a Semidistributed Hydrological Model, Water Resources Research, 55, 8821–8839, https://doi.org/10.1029/2018WR024266, 2019.

Douinot, A., Roux, H., Garambois, P.-A., Larnier, K., Labat, D., and Dartus, D.: Accounting for rainfall systematic spatial variability in flash flood forecasting, Journal of Hydrology, 541, 359–370, 2016.

Douinot, A., Roux, H., Garambois, P.-A., and Dartus, D.: Using a multi-hypothesis framework to improve the understanding of flow dynamics during flash floods, Hydrology and Earth System Sciences, 22, 5317–5340, 2018.

Drobinski, P., Ducrocq, V., Alpert, P., Anagnostou, E., Béranger, K., Borga, M., Braud, I., Chanzy, A., Davolio, S., Delrieu, G., Estournel, C., Boubrahmi, N. F., Font, J., Grubišić, V., Gualdi, S., Homar, V., Ivančan-Picek, B., Kottmeier, C., Kotroni, V., Lagouvardos, K., Lionello, P., Llasat, M. C., Ludwig, W., Lutoff, C., Mariotti, A., Richard, E., Romero, R., Rotunno, R., Roussot, O., Ruin, I., Somot, S., Taupier-Letage, I., Tintore, J., Uijlenhoet, R., and Wernli, H.: HyMeX: A 10-Year Multidisciplinary Program on the Mediterranean Water Cycle, Bulletin of the American Meteorological Society, 95, 1063–1082, https://doi.org/10.1175/BAMS-D-12-00242.1, https://doi.org/10.1175/BAMS-D-12-00242.1, 2014.

Ducrocq, V., Davolio, S., Ferretti, R., Flamant, C., Santaner, V. H., Kalthoff, N., Richard, E., and Wernli, H.: Introduction to the HyMeX Special Issue on 'Advances in understanding and forecasting of heavy precipitation in the Mediterranean through the HyMeX SOP1 field campaign', Quarterly Journal of the Royal Meteorological Society, 142, 1–6, https://doi.org/10.1002/qj.2856, 2016.

Edijatno: Mise au point d'un modèle élémentaire pluie-débit au pas de temps journalier, Ph.D. thesis, Université Louis Pasteur, ENGEES, Cemagref Antony, France, https://webgr.inrae.fr/wp-content/uploads/2012/07/1991-EDIJATNO-THESE.pdf, 1991.

Errico, R. M.: What is an adjoint model?, Bulletin of the American Meteorological Society, 78, 2577–2591, 1997.

Ficchì, A., Perrin, C., and Andréassian, V.: Impact of temporal resolution of inputs on hydrological model performance: An analysis based on 2400 flood events, Journal of Hydrology, 538, 454–470, https://doi.org/https://doi.org/10.1016/j.jhydrol.2016.04.016, http://www.sciencedirect.com/science/article/pii/S0022169416301974, 2016.

Ficchì, A., Raso, L., Dorchies, D., Pianosi, F., Malaterre, P.-O., Overloop, P.-J. V., and Jay-Allemand, M.: Optimal Operation of the Multireservoir System in the Seine River Basin Using Deterministic and Ensemble Forecasts, Journal of Water Resources Planning and Management, 142, 05015 005, https://doi.org/10.1061/(ASCE)WR.1943-5452.0000571, https://ascelibrary.org/doi/abs/10.1061/%28ASCE%29WR.1943-5452.0000571, 2016.

Garambois, P.-A., Roux, H., Larnier, K., Castaings, W., and Dartus, D.: Characterization of process-oriented hydrologic model behavior with temporal sensitivity analysis for flash floods in Mediterranean catchments, Hydrology and Earth System Sciences, 17, 2305–2322, 2013.

Garambois, P.-A., Roux, H., Larnier, K., Labat, D., and Dartus, D.: Parameter regionalization for a process-oriented distributed model dedicated to flash floods, Journal of Hydrology, 525, 383–399, 2015.

Gourley, J., Flamig, Z., Vergara, H., Kirstetter, P.-E., Clark, R., Argyle, E., Arthur, A., Martinaitis, S., Terti, G., Erlingis, J., Hong, Y., and Howard, K.: The flash project Improving the Tools for Flash Flood Monitoring and Prediction across the United States, Bulletin of the American Meteorological Society, 98, 361–372, https://doi.org/10.1175/BAMS-D-15-00247.1, 2017.

Gupta, H. V., Kling, H., Yilmaz, K. K., and Martinez, G. F.: Decomposition of the mean squared error and NSE performance criteria: Implications for improving hydrological modelling, Journal of Hydrology, Volume 377, Issue 1, p. 80-91., 377, 80–91, https://doi.org/10.1016/j.jhydrol.2009.08.003, 2009.

Hapuarachchi, H., Wang, Q., and Pagano, T.: A review of advances in flash flood forecasting, Hydrological Processes, 25, 2771–2784, https://doi.org/10.1002/hyp.8040, 2011.

Hascoet, L. and Pascual, V.: The Tapenade Automatic Differentiation tool: principles, model, and specification, ACM Transactions on Mathematical Software (TOMS), 39, 20, 2013.

Javelle, P., Fouchier, C., Arnaud, P., and Lavabre, J.: Flash flood warning at ungauged locations using radar rainfall and antecedent soil moisture estimations, Journal of Hydrology, 394, 267–274, 2010.

Javelle, P., Demargne, J., Defrance, D., Pansu, J., and Arnaud, P.: Evaluating flash-flood warnings at ungauged locations using post-event surveys: a case study with the AIGA warning system, Hydrological sciences journal, 59, 1390–1402, 2014.

Javelle, P., Organde, D., Demargne, J., Saint-Martin, C., de Saint-Aubin, C., Garandeau, L., and Janet, B.: Setting up a French national flash flood warning system for ungauged catchments based on the AIGA method, in: 3rd European Conference on Flood Risk Management FLOODrisk 2016, vol. 7, p. 11, 2016.

Javelle, P., Saint-Martin, C., Garandeau, L., and Janet, B.: Flash flood warnings: Recent achievements in France with the national Vigicrues Flash system., United Nations Office for Disaster Risk Reduction, Contributing Paper to the Global Assessment Report on Disaster Risk Reduction (GAR 2019), https://www.undrr.org/publication/flash-flood-warnings-recent-achievements-france-national-vigicrues-flash-system, 2019.

Jay-Allemand, M., Gejadze, I., Javelle, P., Organde, D., Fine, J.-A., Patrick, A., and Malaterre, P.-O.: Assimilation de données appliquée à un modèle pluie-débit distribué pour la prévision des crues, in: De la prévision des crues à la gestion de crise, Société hydaulique de France, Avignon, 2018.

Klemes, V.: Operational testing of hydrological simulation models, Hydrological Sciences Journal, 31, 13–24, https://doi.org/10.1080/02626668609491024, 1986.

Laganier, O., Ayral, P. A., Salze, D., and Sauvagnargues, S.: A coupling of hydrologic and hydraulic models appropriate for the fast floods of the Gardon River basin (France), Natural Hazards and Earth System Sciences, 14, 2899–2920, 2014.

Laurent, L., Le Riche, R., Soulier, B., and Boucard, P.-A.: An Overview of Gradient-Enhanced Metamodels with Applications, Archives of Computational Methods in Engineering, 26, 61–106, 2019.

Ledimet, F. and Talagrand, O.: Variational Algorithms For Analysis And Assimilation Of Meteorological Observations - Theoretical Aspects, Tellus Series A-Dynamic Meteorology And Oceanography, 38, 97–110, https://doi.org/10.3402/tellusa.v38i2.11706, 1986.

Lee, H., Seo, D. J., Liu, Y., Koren, V., McKee, P., and Corby, R.: Variational assimilation of streamflow into operational distributed hydrologic models: effect of spatiotemporal scale of adjustment, Hydrology and Earth System Sciences, Volume 16, Issue 7, 2012, pp.2233-2251, 16, 2233–2251, https://doi.org/10.5194/hess-16-2233-2012, 2012.

Liu, Y., Weerts, A. H., Clark, M., Hendricks Franssen, H.-J., Kumar, S., Moradkhani, H., Seo, D.-J., Schwanenberg, D., Smith, P., van Dijk, A. I. J. M., van Velzen, N., He, M., Lee, H., Noh, S. J., Rakovec, O., and Restrepo, P.: Advancing data assimilation in operational hydrologic forecasting: progresses, challenges, and emerging opportunities, Hydrology and Earth System Sciences, Volume 16, Issue 10, 2012, pp.3863-3887, 16, 3863–3887, https://doi.org/10.5194/hess-16-3863-2012, 2012.

Lobligeois, F., Andréassian, V., Perrin, C., Tabary, P., and Loumagne, C.: When does higher spatial resolution rainfall information improve streamflow simulation?: An evaluation using 3620 flood events, Hydrology and Earth System Sciences, Volume 18, Issue 2, 2014, pp.575-594, 18, 575–594, https://doi.org/10.5194/hess-18-575-2014, 2014.

McLaughlin, D.: Recent developments in hydrologic data assimilation, Reviews of Geophysics, 33, 977–984, 1995.

Moradkhani, H. and Sorooshian, S.: General review of rainfall-runoff modeling: model calibration, data assimilation, and uncertainty analysis, in: Hydrological modelling and the water cycle, pp. 1–24, Springer, 2009.

Mouelhi, S., Michel, C., Perrin, C., and Andréassian, V.: Linking stream flow to rainfall at the annual time step: the Manabe bucket model revisited, Journal of hydrology, 328, 283–296, 2006.

Munier, S., Litrico, X., Belaud, G., and Perrin, C.: Assimilation of discharge data into semidistributed catchment models for short-term flow forecasting: Case study of the Seine River basin, Journal of Hydrologic Engineering, 20, 05014 021, 2014.

Nash, J. E. and Sutcliffe, J. V.: River flow forecasting through conceptual models. Part I. A conceptual models discussion of principles., Journal of Hydrology, 10, 282–290, 1970.

Nguyen, V. T., Georges, D., Besançon, G., and Zin, I.: Parameter estimation of a real hydrological system using an adjoint method, IFAC-PapersOnLine, 49, 300–305, https://doi.org/10.1016/j.ifacol.2016.07.978, 2016.

Oudin, L., Hervieu, F., Michel, C., Perrin, C., Andréassian, V., Anctil, F., and Loumagne, C.: Which potential evapotranspiration input for a lumped rainfall–runoff model?: Part 2—Towards a simple and efficient potential evapotranspiration model for rainfall–runoff modelling, Journal of hydrology, 303, 290–306, 2005.

Perrin, C., Michel, C., and Andréassian, V.: Improvement of a parsimonious model for streamflow simulation, Journal of Hydrology, Volume 279, Issue 1, p. 275-289., 279, 275–289, https://doi.org/10.1016/S0022-1694(03)00225-7, 2003.

Pokhrel, P. and Gupta, H. V.: On the use of spatial regularization strategies to improve calibration of distributed watershed models, Water Resources Research, 46, 2010.

Quesney, A., Francois, C., Ottle, C., Hegarat, S., Loumagne, C., Normand, M., et al.: Sequential assimilation of SAR/ERS data in a lumped rainfall-runoff model with an extended Kalman filter, IAHS-AISH PUBL., pp. 495–497, 2000.

Rabier, F. and Courtier, P.: Four-dimensional assimilation in the presence of baroclinic instability, Quart. J. Roy. Meteorol. Soc., 118, 649–672, 1992.

Rakovec, O., Kumar, R., Attinger, S., and Samaniego, L.: Improving the realism of hydrologic model functioning through multivariate parameter estimation, Water Resources Research, 52, 7779–7792, www.scopus.com, 2016.

Riboust, P., Thirel, G., Moine, N. L., and Ribstein, P.: Revisiting a Simple Degree-Day Model for Integrating Satellite Data: Implementation of Swe-Sca Hystereses, Journal of Hydrology and Hydromechanics, 67, 70–81, 2019.

Roux, H., Labat, D., Garambois, P. A., Maubourguet, M. M., Chorda, J., and Dartus, D.: A physically-based parsimonious hydrological model for flash floods in Mediterranean catchments, Natural Hazards and Earth System Science, 11, 2567–2582, https://doi.org/10.5194/nhess-11-2567-2011, 2011.

Samaniego, L., Kumar, R., and Attinger, S.: Multiscale parameter regionalization of a grid-based hydrologic model at the mesoscale, Water Resources Research, 46, https://doi.org/10.1029/2008WR007327, 2010.

Santos, L., Thirel, G., and Perrin, C.: Continuous state-space representation of a bucket-type rainfall-runoff model: a case study with the GR4 model using state-space GR4 (version 1.0), Geoscientific Model Development, 11, 1591–1605, 2018.

Seo, D.-J., Cajina, L., Corby, R., and Howieson, T.: Automatic state updating for operational streamflow forecasting via variational data assimilation, Journal of Hydrology, Volume 367, Issue 3, p. 255-275., 367, 255–275, https://doi.org/10.1016/j.jhydrol.2009.01.019, 2009.

Sun, L., Nistor, I., and Seidou, O.: Streamflow data assimilation in SWAT model using Extended Kalman Filter, Journal of Hydrology, 531, 671–684, 2015.

Sun, L., Seidou, O., Nistor, I., and Liu, K.: Review of the Kalman-type hydrological data assimilation, Hydrological Sciences Journal, 61, 2348–2366, 2016.

Thirel, G., Martin, E., Mahfouf, J. F., Massart, S., Ricci, S., and Habets, F.: A past discharges assimilation system for ensemble streamflow forecasts over France–Part 1: Description and validation of the assimilation system, Hydrology and Earth System Sciences, 14, 1623–1637, 2010.

Tramblay, Y., Bouvier, C., Crespy, A., and Marchandise, A.: Improvement of flash flood modelling using spatial patterns of rainfall: A case study in southern France, pp. 172–178, 2010.

Vannier, O., Braud, I., and Anquetin, S.: Regional estimation of catchment-scale soil properties by means of streamflow recession analysis for use in distributed hydrological models, Hydrological Processes, 28, 6276–6291, https://doi.org/10.1002/hyp.10101, 2014.

Vannier, O., Anquetin, S., and Braud, I.: Investigating the role of geology in the hydrological response of Mediterranean catchments prone to flash-floods: Regional modelling study and process understanding, Journal of Hydrology, 541, 158–172, https://doi.org/10.1016/j.jhydrol.2016.04.001, 2016.

Vidal, J. P., Martin, E., Franchistéguy, L., Baillon, M., and Soubeyroux, J. M.: A 50-year high-resolution atmospheric reanalysis over France with the Safran system, International Journal of Climatology, 30, 1627–1644, https://doi.org/10.1002/joc.2003, 2010.

Wang, J., Hong, Y., Li, L., Gourley, J. J., Khan, S. I., Yilmaz, K. K., Adler, R. F., Policelli, F. S., Habib, S., Irwn, D., et al.: The coupled routing and excess storage (CREST) distributed hydrological model, Hydrological sciences journal, 56, 84–98, 2011.

Zhu, C., Byrd, R. H., Lu, P., and Nocedal, J.: L-BFGS-B: a limited memory FORTRAN code for solving bound constrained optimization problems, EECS Department, Northwestern University, Evanston, IL, Technical Report No. NAM-11, 1994.
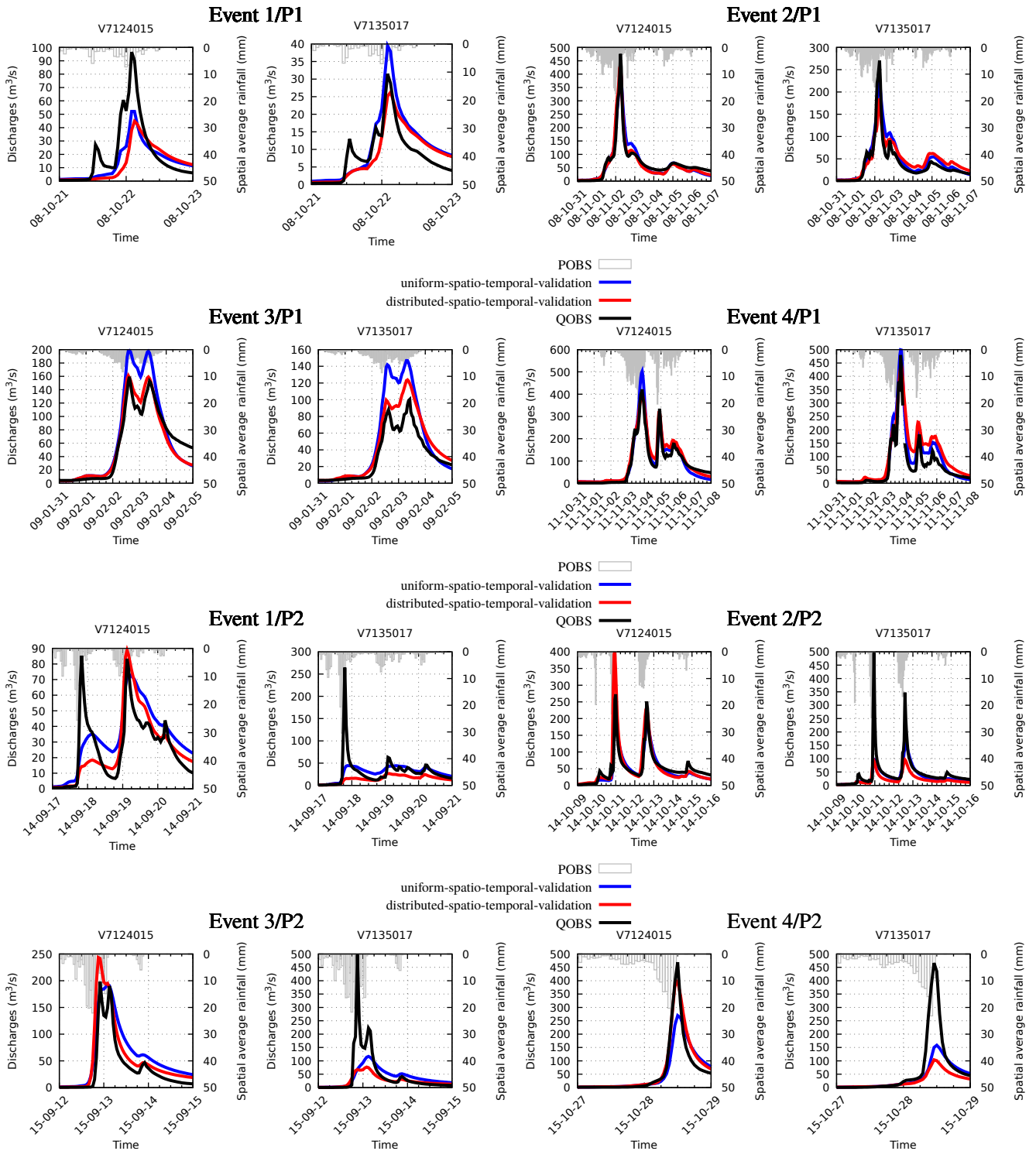
Figure 5. Spatio-temporal predicted discharges (with the distributed and uniform set of parameters) and observed discharges during the height majors events issued from period P1 and P2 at stations V7124015 and V7135017.
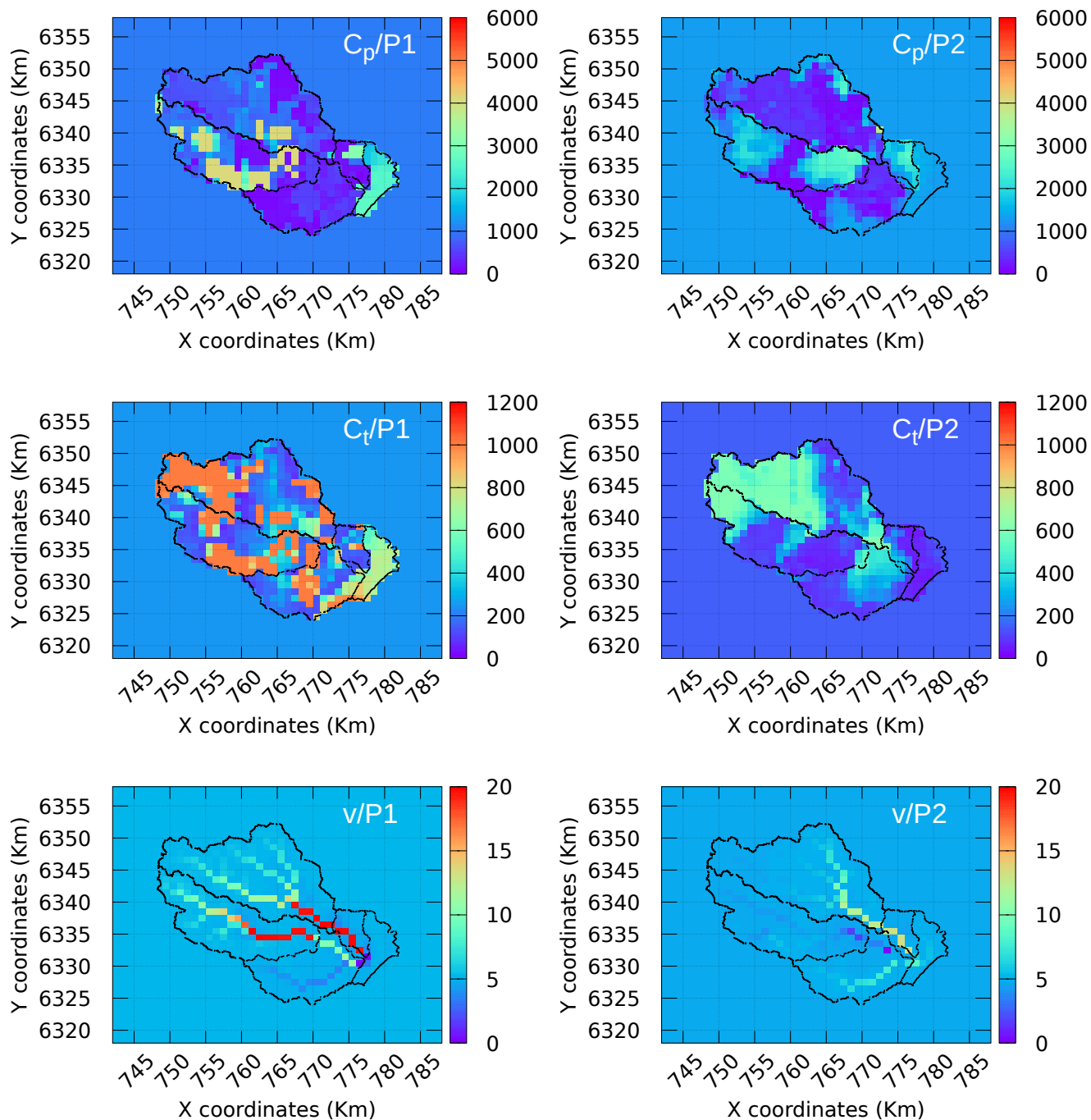
Figure 6. Maps of the calibrated coefficients (exp.1 - 5-sta): left - data from $P1$, right - data from $P2$.
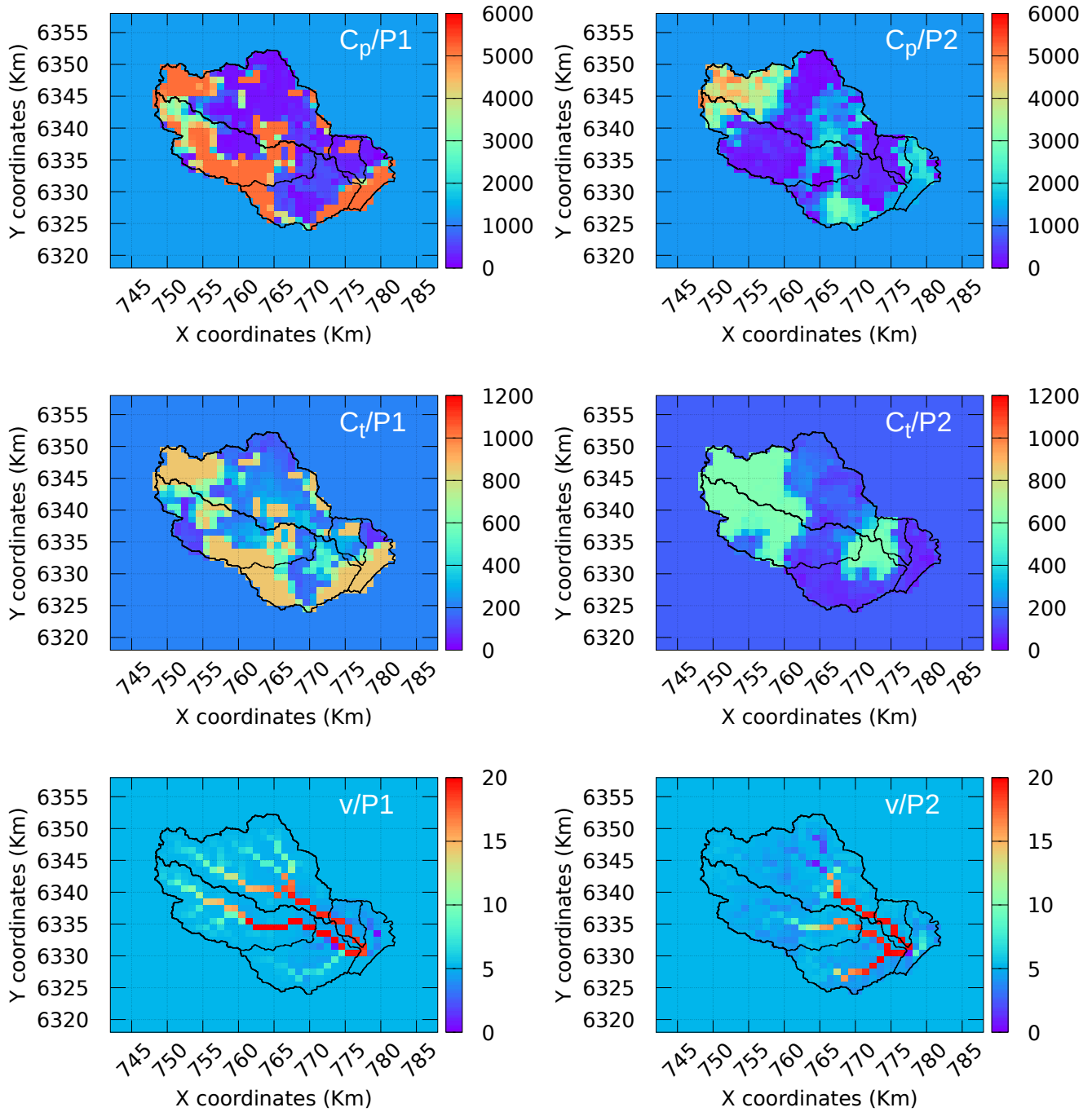
Figure 7. Maps of the calibrated coefficients (exp.3 - 1-sta): left - data from $P1$, right - data from $P2$.
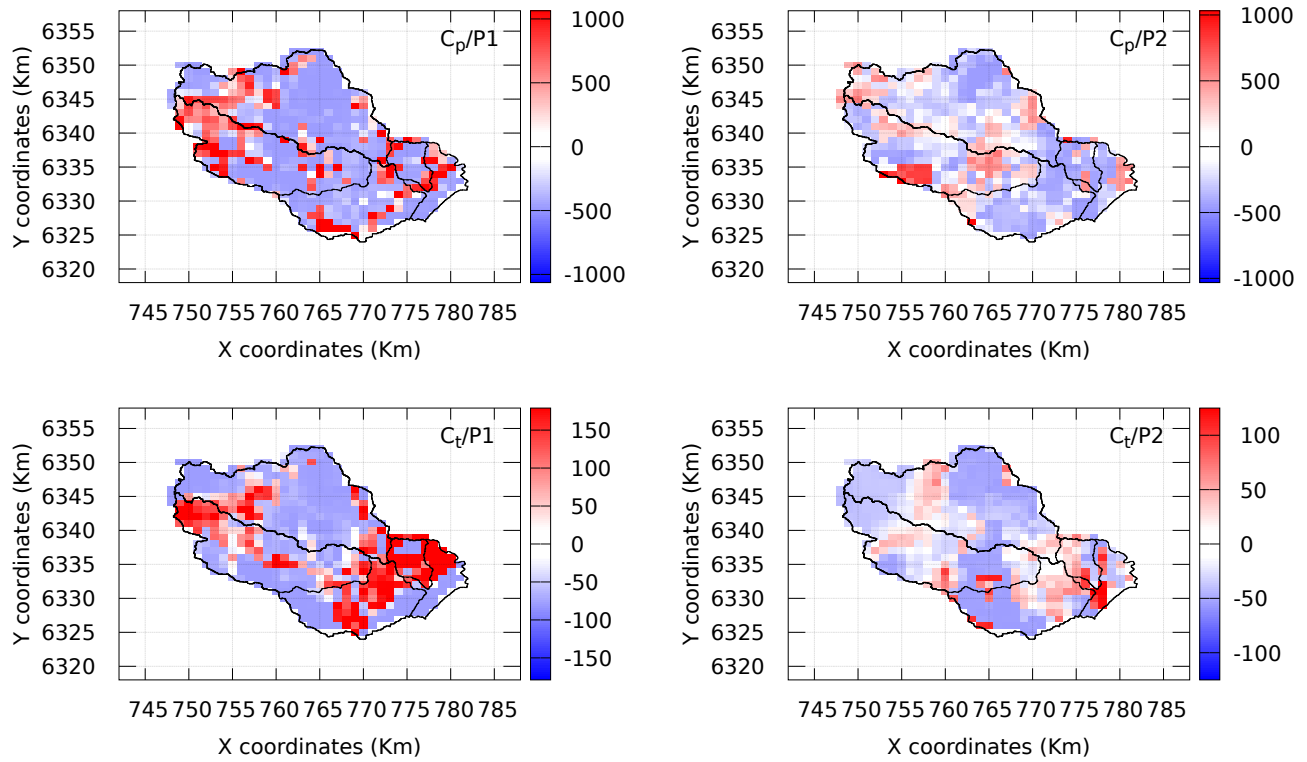
Figure 8. Maps of stability measure σ_θ for: c_p (upper) and c_t (lower), for periods $P1$ (left) and $P2$ (right)